

## Energetics and kinetics unveiled on helium cluster growth in tungsten

This content has been downloaded from IOPscience. Please scroll down to see the full text.

2015 Nucl. Fusion 55 092003

(<http://iopscience.iop.org/0029-5515/55/9/092003>)

View [the table of contents for this issue](#), or go to the [journal homepage](#) for more

Download details:

IP Address: 69.62.157.224

This content was downloaded on 12/09/2015 at 14:44

Please note that [terms and conditions apply](#).

## Letter

# Energetics and kinetics unveiled on helium cluster growth in tungsten

Jinlong Wang, Liang-Liang Niu, Xiaolin Shu and Ying Zhang

Department of Physics, Beihang University, Beijing 100191, People's Republic of China

E-mail: [zhyi@buaa.edu.cn](mailto:zhyi@buaa.edu.cn)

Received 20 April 2015, revised 29 May 2015

Accepted for publication 3 July 2015

Published 20 August 2015

**Abstract**

The energetics and kinetics regarding helium (He) cluster growth in bcc tungsten (W) are unveiled using combined techniques of molecular statics and molecular dynamics. The principal mechanisms accounting for the decrease of system potential energy are identified to be trap mutation,  $\langle 100 \rangle \rightarrow 1/2\langle 111 \rangle$  cluster transformation, loop punching, coalescence between  $1/2[1\ 1\ -1]$  and  $1/2[1\ -1\ -1]$  loops, and loop capturing. The kinetic barriers associated with these key atomistic events are estimated. This work provides new insights into the complex yet intriguing atomistic evolution sequence of the He cluster and interstitial loop in W-based nuclear fusion materials under irradiation.

Keywords: helium cluster growth, energies, kinetics, loop capturing

(Some figures may appear in colour only in the online journal)

The behavior of helium (He) in metals has been a subject of both scientific interest and technological significance for decades [1–9]. Because of its extremely low solubility, high mobility and self-trapping characters, substantial amounts of He, produced whether via  $(n, \alpha)$  transmutation reaction or via direct He plasma implantation, can easily migrate and aggregate at various defect sinks [10–13], leading to the nucleation and growth of He clusters, thus seriously degrading the physical and mechanical properties [14–17] of the leading candidate for plasma facing materials (PFMs), tungsten (W), in future nuclear fusion reactors. Experimentally, He blisters and so called ‘fuzz’ nanostructures [16, 18–22] have been observed on the W surface under He-ion irradiation at intermediate temperatures. Prior studies [23, 24] demonstrated that the nucleation of He clusters can proceed via a trap mutation process without pre-existing vacancies. Further growth of the He cluster involves loop punching, as evidenced by transmission electronic microscopy (TEM) [25]. At high temperatures, cluster coalescence provides another route for cluster growth due to the augmented mobility of He clusters [21]. Nonetheless, the nanoscale He clusters at their early stages go beyond the resolution of TEM; therefore, alternative

approaches are imperative to shed light onto the He behavior in metals.

Atomistic simulations have captured the attention of the materials science community for not only validating experimental observations but providing new insight into the underlying mechanisms governing many physical processes in materials and predicting material behavior under a wide range of situations, which may be unattainable via experimental techniques. To date, extensive simulation works have covered the dissolution, migration and clustering behaviors of He in metals. Using first-principles calculations, Seletskaja *et al* [2] demonstrated that He is energetically favorable to occupy the tetrahedral interstitial site (TIS) in bcc transition metals and its formation energies are strongly influenced by the electronic structure of the host metals. Becquart *et al* [4] reported that the migration barrier of He in W is as low as 0.06 eV. In terms of the dynamic behaviors of cluster nucleation and growth, a series of atomistic simulations have been conducted to investigate the evolution of He clusters in titanium [26], iron [27] and W [6, 28], revealing that He cluster growth is accompanied by the trap mutation and loop punching events. Despite the valuable resources provided by these earlier studies,

a comprehensive understanding on the evolution of He clusters in W at its early stages is still lacking due to the technological difficulties in observing these dynamic processes.

Here we reveal the microscopic mechanisms of He cluster nucleation and growth in bulk W regarding its energetics and kinetics using combined techniques of molecular statics (MS) and molecular dynamics (MD). A parallel MD package, LAMMPS [29], is utilized in all simulations. The interatomic potential is described in detail in [30]. A large cubic simulation cell of  $24a \times 24a \times 24a$  (27648 atoms) is constructed to eliminate the possible size effect, where the lattice constant  $a$  is 3.168 Å at 300 K. Periodic boundary conditions are used in all 3D. Initially, a He<sub>5</sub> cluster (low mobility) was inserted into the interstitial site at the center of the supercell. Subsequently, He atoms were introduced one by one into the center of the mass of the pre-existing He cluster, followed by an energy minimization in which only the newly-inserted atom was allowed to relax to avoid overlapping. We set the initial velocity of the inserted He to zero, then control the temperature of the system to 300 K using the Nose–Hoover thermostat [31–33]. The time span between neighboring He insertions was over 30 ps. An adaptable time step was utilized with each time step ranging from  $10^{-4}$  ps to  $10^{-3}$  ps. Three independent simulations were separately run up to ~10 ns to attain reasonable statistics and structure visualization was done by OVITO [34], while the ‘Wigner-Seitz analysis’ code implemented in OVITO was employed for Frenkel pair examination.

For each cluster size, energetics analysis is accomplished by means of MD relaxations at 300 K, followed by an energy minimization to obtain the configuration-dependent binding energies. This approach dramatically increases the probability of the system to find global minima. The total binding energy of the He cluster is calculated by

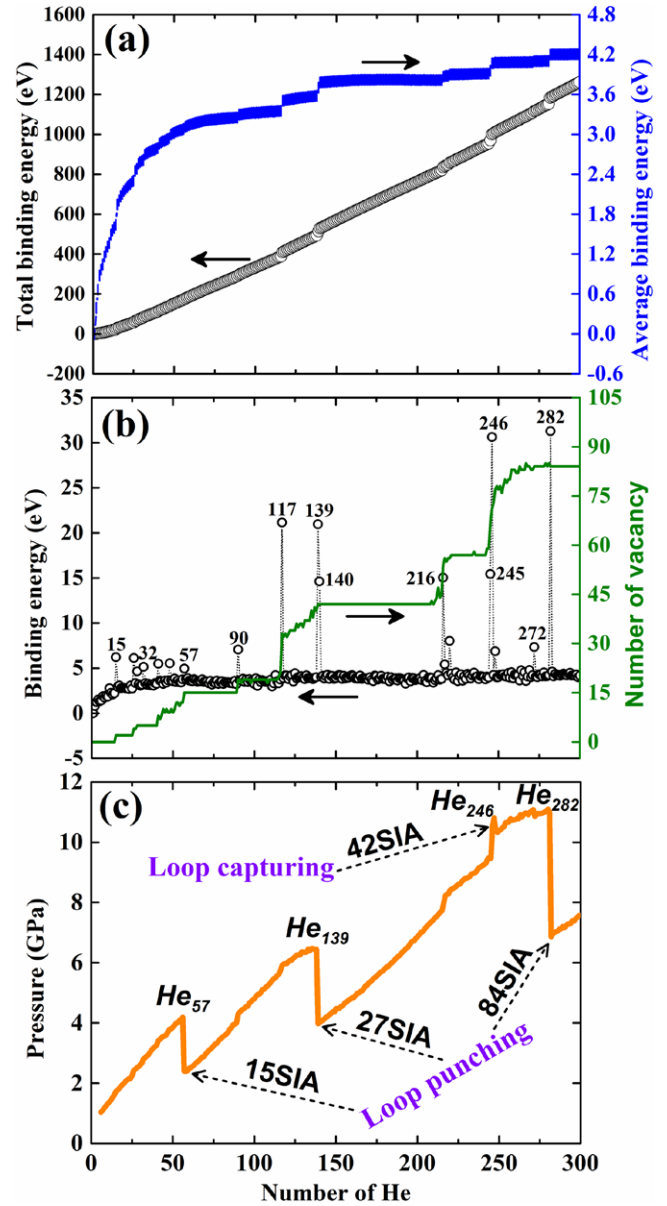
$$E^b(\text{He}_n) = nE^f(\text{He}_{\text{TIS}}) - E^f(\text{He}_n), \quad (1)$$

where  $E^f(\text{He}_n)$  is the formation energy of the He<sub>n</sub> cluster and  $E^f(\text{He}_{\text{TIS}})$  is the formation energy of a single He located at the tetrahedral interstitial site in the bulk. Naturally, the average binding energy can be simply expressed as  $E^b(\text{He}_n)/n$ . The binding energy between a single He with a He<sub>n-1</sub> cluster is defined as

$$E^b(\text{He} - \text{He}_{n-1}) = E^f(\text{He}_{n-1}) + E^f(\text{He}_{\text{TIS}}) - E^f(\text{He}_n), \quad (2)$$

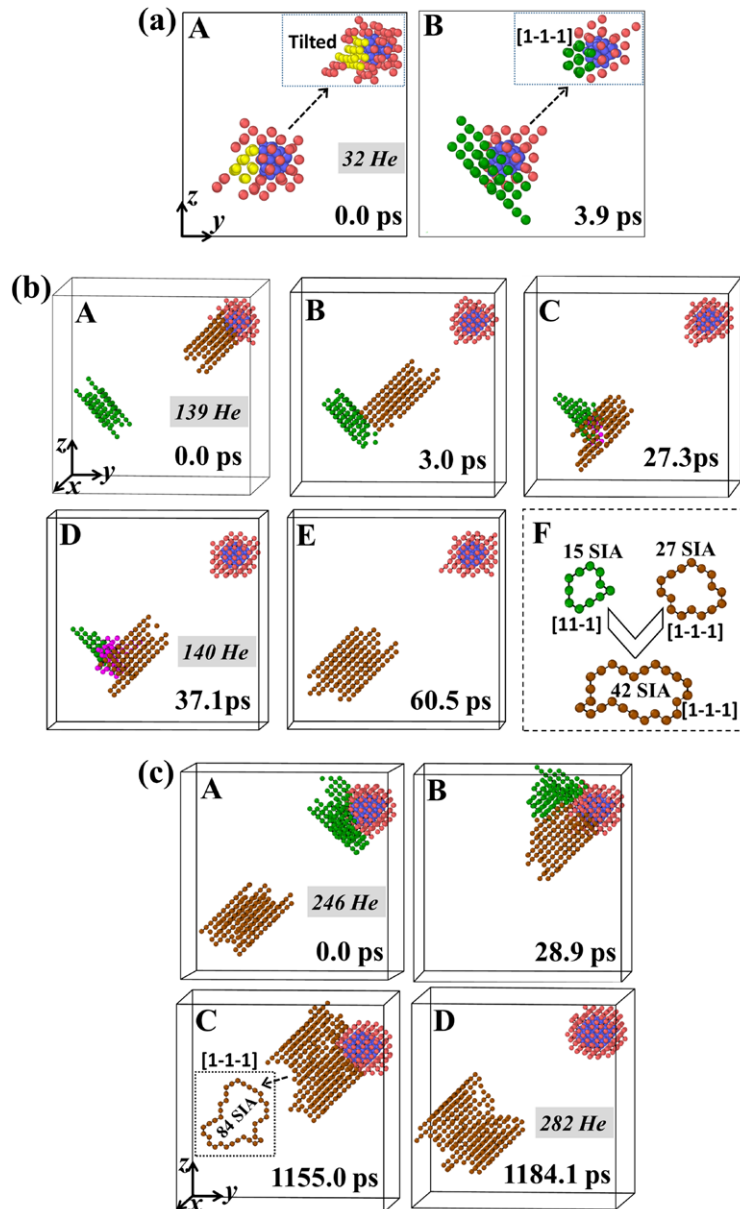
where  $E^f(\text{He}_{n-1})$  and  $E^f(\text{He}_n)$  are the formation energies of a He<sub>n-1</sub> and He<sub>n</sub> cluster in the bulk, respectively. Note that pressure (or stress) is an effective indicator for certain critical events occurring in the cluster growth process. Since it is difficult to define the volume of the small He clusters due to its irregular shape, we directly calculated the pressure of a spherical region (with a radius of  $7a$ , centering at the center of mass of the He cluster) encompassing the He cluster. Considering the thermal fluctuations, the pressure was time-averaged within the next 5 ps after thermal equilibrium.

Figure 1 presents the total and average binding energies of He<sub>n</sub> clusters ( $1 \leq n \leq 300$ ) as a function of cluster size. The total binding energy of the He cluster displays an approximately linear increase with increasing He cluster size; while the average binding energy increases rapidly at the initial



**Figure 1.** (a) Total and average binding energy as a function of cluster size. (b) Binding energy between a single He and a He<sub>n-1</sub> cluster and vacancy number as a function of cluster size. Pronounced energy peaks are labelled by the corresponding He number. (c) Pressure of the spherical region encompassing the He cluster. The sharp drops correspond to loop punching events, while the sharp rise denotes loop capturing.

stage, but slows down at larger cluster sizes. These results demonstrate that self-trapping is energetically favorable for He in W. Small He<sub>n</sub> ( $4 \leq n \leq 14$ ) clusters were found to assume three-dimensional (3D) structures and form a platelet between the close-packed (110) planes, consistent with the earlier TEM study in molybdenum [35]. Continuous capturing of He atoms leads to trap-mutation at a critical size of He<sub>15</sub>, creating 2 Frenkel pairs. The He cluster penetrates through the restraint of one (110) plane and trends towards a spherical morphology. Due to the thermal fluctuations, we also observed the initiation of this process for the He<sub>13</sub> or He<sub>14</sub> case in other simulations, in good agreement with [36], in which trap mutation can be readily detected at 300 K using the same



**Figure 2.** (a) Snapshots for the rotation of a  $\langle 100 \rangle$  SIA cluster into a  $1/2\langle 111 \rangle$  loop. The atoms are magnified for visual clarity. (b) A-E are a sequence of snapshots for the loop reaction and coalescence and F is a complementary image viewed from the orientation of the corresponding loops for better understanding of this process. (c) Snapshots for the sequential occurrence of loop capturing, loop coalescence and loop punching events. The beginning time for each evolution process is set to zero to facilitate easy comparison, and their time references are 1.11, 4.78 and 8.27 ns, respectively. The  $[100]$ ,  $1/2[1-1-1]$  and  $1/2[1-1-1]$  cluster or loops are colored yellow, green and brown, respectively. The He atoms are colored blue and the other W atoms are colored pink and only atoms with higher energy of 0.3 eV than the bulk are shown.

potential. Interestingly, both curves in figure 1(a) show sharp rises at certain cluster sizes. In order to gain more insight into the underlying mechanism of cluster growth in terms of its energetics, we plot in figure 1(b) the binding energy between the  $n$ th He and a  $\text{He}_{n-1}$  cluster and the number of vacancies with growing He cluster. The binding energy exhibits a number of peaks with most of them corresponding to the instantaneous climb of vacancy number (trap mutation), which has been evidenced to be an important mechanism for the nucleation and growth of He clusters [37]. For instance, the addition of 117th He induces a sharp energy peak due to the collective trap mutation events (creating 12 Frenkel pairs) and the

subsequent absorption of the 12 SIAs by the pre-existing SIA loop attached to the He cluster. Surprisingly, several energy peaks during the cluster evolution process cannot be related to trap mutation. Identification of alternative mechanisms is required to account for these abnormalities.

To understand the possible origin of these phenomena, following a chronological order, we next explore the critical events occurring in the He cluster growth process. In figure 1(b), the energy peak at  $\text{He}_{32}$  cannot be explained by the trap mutation process. Figure 2(a) illustrates the evolution sequence upon the addition of the 32nd He into the cluster. At 0.0 ps (time reference 1.11 ns), a small  $\langle 100 \rangle$  SIA cluster

containing 5 SIAs, formed due to the repeated trap mutation processes, is pinned by the He cluster. At 3.9 ps, the  $\langle 100 \rangle$  SIA cluster reorientates to a more stable  $1/2\langle 111 \rangle$  SIA loop, thus relieving the large distortion energy of the system. From this point, the  $1/2\langle 111 \rangle$  loop continues to absorb newly generated SIAs as the He cluster grows, resulting in its ultimate emission.

Energetics analysis is capable of reflecting a wide range of physical processes. Nevertheless, sometimes the individual features of these processes cannot be fully captured. To complement this approach, we plot in figure 1(c) the pressure of a spherical region with He cluster size to further reveal the critical events in the cluster evolution process. Here the pressure is not sensitive to the trap mutation and the cluster transformation processes taking place inside the spherical region, but it allows for the distinct detection of loop punching and loop capturing events. In fact, the SIA loops pinned by the He cluster are always inside the spherical region, whereas they escape from this region, turning into free loops, once a critical pressure is reached. Conversely, the free loops can also be absorbed into the spherical region and pinned by the He cluster through a new mechanism called ‘loop capturing’, which we will illustrate later in detail. Take He<sub>57</sub> for example, a  $1/2\langle 111 \rangle$  loop containing 15 SIAs tears away from the He cluster along the  $[1\ 1\ -1]$  direction, resulting in a pressure drop of  $\sim 1.8$  GPa (as shown in figure 1(c)). Due to the stochastic nature of these events, in the other two simulations, the first loop punching event occurs when the 46th and 51st He are introduced into the He cluster, respectively.

Interestingly, as shown in figure 1(b), two successive peaks arise at He<sub>139</sub> and He<sub>140</sub> involving no pronounced Frenkel pair creation. To resolve this puzzle, figure 2(b) presents a sequence of snapshots from the MD simulations at 300 K. At 0.0 ps (time reference 4.78 ns), a  $1/2[1\ -1\ -1]$  SIA loop containing 27 SIAs is on the edge of emission; at 3.0 ps, loop punching occurs, inducing a sharper pressure drop of  $\sim 2.3$  GPa (see figure 1(c)). The loop subsequently undergoes 1D fast migration towards the precedent  $1/2[1\ 1\ -1]$  loop. Their collision leads to the formation of a sessile junction (see figure 2(b) C and D), which is vital for the individual SIAs to interact, overcoming an array of kinetic barriers along the reaction coordinate. The driving force of this reaction is the considerable reduction of loop energy associated with loop condensation. At 60.5 ps, the condensation is completed, forming a larger  $1/2\langle 111 \rangle$  loop containing 42 SIAs. Unlike a recent SIA loop study in bcc iron using the kinetic Monte Carlo method [38], in which the formation of a  $\langle 100 \rangle$  loop resulting from two interacting  $1/2\langle 111 \rangle$  loops occurs at the timescale of microseconds, the loop reaction and coalescence here can be readily completed within the timescale of MD ( $\sim 10$  ns). Furthermore, consistent with [39], it is kinetically favorable for the smaller loop to rotate and coalesce with the larger one, contributing to the loop growth. We emphasize that the loops encounter because of the periodic boundary conditions. However, in real situations, when a high number density of He clusters is present, this phenomenon is expected to occur frequently.

With the further growth of the He cluster, figure 1(b) shows that, following the concomitant energy peak and sharp

vacancy increase at He<sub>245</sub>, a higher energy peak emerges at He<sub>246</sub>. Figure 2(c) presents a sequence of MD snapshots for this complex evolution sequence beginning upon the addition of the 246th He. At 0.0 ps (time reference 8.27 ns), the SIA loop with orientation  $1/2[1\ -1\ -1]$  containing 42 SIAs is far away from the He cluster, while the other SIA loop with  $1/2[1\ 1\ -1]$  orientation, formed during cluster growth from He<sub>140</sub> to He<sub>246</sub>, is pinned by the He cluster. At 28.9 ps, the free loop quickly glides towards the He cluster and attaches to it, inducing a sharp pressure rise (see figure 1(c)). We thus name this process ‘loop capturing’. Energetically, the system is greatly stabilized after this process (indicated by the high energy peak at He<sub>246</sub> in figure 1(b)), possibly due to the strong attraction between the two loops. Within the next  $\sim 1$  ns, trap mutation continues to occur, meanwhile, the two  $1/2\langle 111 \rangle$  loops begin to react and coalesce, following a similar evolution sequence as figure 2(b). This loop coalescence sequence is completed at 1155.0 ps (corresponding to the addition of the 282th He), after which a major loop punching of a large  $1/2\langle 111 \rangle$  loop containing 84 SIAs occurs at 1184.1 ps, corresponding to a dramatic pressure drop of  $\sim 4$  GPa (as shown in figure 1(c)). We stress that the number of SIAs in the loop and the number of vacancies are always equal after each loop punching events, indicating that no single SIAs exist in the system at that particular moment.

One may wonder why these events can be observed within the limited timescale of MD. It is well recognized that the rate at which these physical processes occur is governed by their kinetic behaviors. Therefore, in an attempt to shed light onto the kinetics underlying He cluster growth, we assess the barriers for some of the critical events using nudged elastic band (NEB) method [40]. Notably, due to the high mobility of He atoms and their complex rearrangement in the cluster, the minimum energy pathway for events such as cluster transformation and loop reaction may not be correctly reflected. We circumvent this difficulty via eliminating or freezing the He cluster to make a rough estimation. For example, the kinetic barrier for the reaction displayed in figure 2(a) is estimated by evaluating the  $\langle 100 \rangle \rightarrow 1/2\langle 111 \rangle$  cluster (5-SIA) transformation process in a perfect lattice without the interference of He cluster. As shown in figure 3(a), it is energetically favorable for the system to evolve from  $\langle 100 \rangle$  cluster to  $1/2\langle 111 \rangle$  cluster with an energy release of 1.12 eV. Kinetically, instead of rotating collectively, the  $\langle 100 \rangle \rightarrow 1/2\langle 111 \rangle$  cluster transformation (see the insets of figure 3(a)) proceeds via the initial reorientation of one  $\langle 100 \rangle$  dumbbell into  $\langle 111 \rangle$  crowdion with a barrier of 0.48 eV, followed by the collective rotation of the other four  $\langle 100 \rangle$  dumbbells into  $\langle 111 \rangle$  crowdions with a tiny barrier of 0.04 eV, while the reverse process  $1/2\langle 111 \rangle \rightarrow \langle 100 \rangle$  cluster transformation has a higher barrier of 1.6 eV. Interestingly, when only 4 SIAs are present, the barrier of  $\langle 100 \rangle \rightarrow 1/2\langle 111 \rangle$  cluster transformation is determined to be as high as 1.21 eV, implying that the prior reorientation of the fifth SIA significantly assists the rotation of the other four.

Further, we plot in figure 3(b) the reaction pathway for loop reaction and coalescence between the  $1/2[1\ 1\ -1]$  and  $1/2[1\ -1\ -1]$  loops, corresponding to the evolution sequence in figure 2(b) from ‘B’ to ‘E’. A sessile junction is immediately

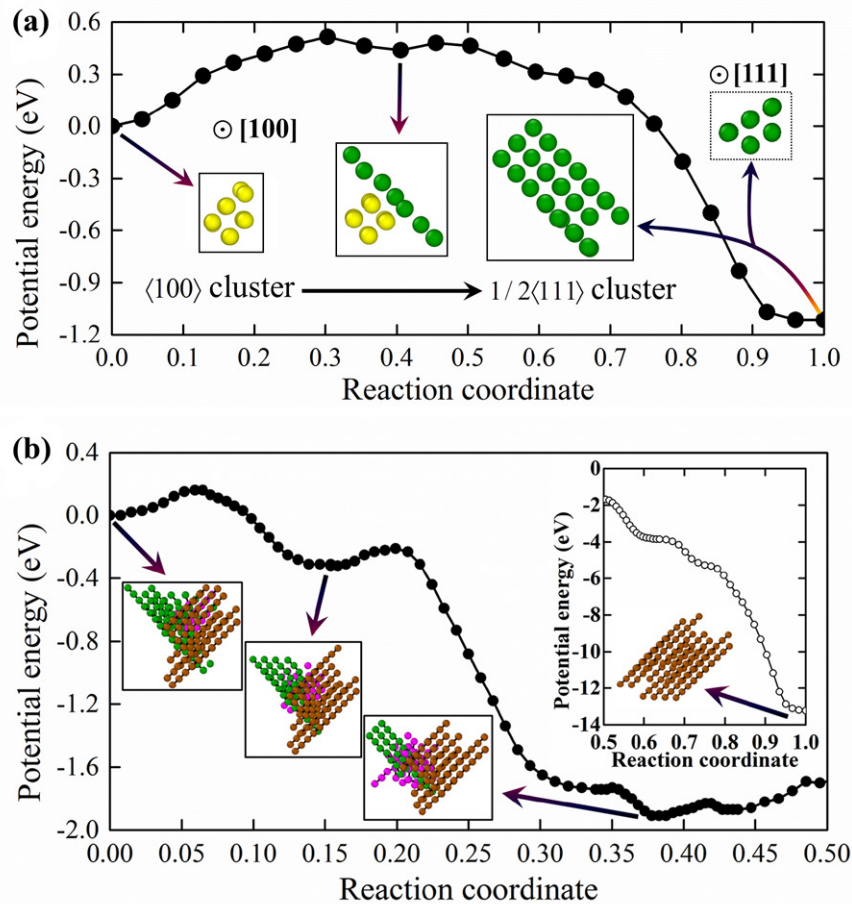


**Figure 3.** (a) Energy landscape of SIA cluster evolution determined by the NEB method. The insets below the reaction pathway are defect configurations at the minima seen from  $[100]$  direction, while the inset above illustrates the final defect configuration seen from  $[111]$  direction. Note that  $\langle 100 \rangle$  dumbbells and  $1/2\langle 111 \rangle$  crowdions are colored yellow and green, respectively. (b) Energy landscape of  $1/2[1-1-1]$  and  $1/2[1-1-1]$  loop reaction and coalescence (see figure 2(b)) determined by NEB method. The coloring scheme and view direction of the defect structures are the same as figure 2(b). Only the loops are shown and the later stage of the evolution is presented as the insets at the upper right corner.

formed upon energy minimization at the early stage, from which the system evolves along a ‘down-hill drift’ route towards coalescence, overcoming a sequential barriers of 0.165, 0.108, 0.014 and 0.191 eV. Specifically, the reaction proceeds via the gradual expansion of the sessile junction and the subsequent transformation of the junction into the orientation of the larger loop, as indicated by the steep energy curve at the latter stage of the reaction pathway (see the inset plot of figure 3(b)). This reaction involves a dramatic energy release of  $\sim 13.5$  eV, confirming the energetics analysis we have made above (see figure 1(b) at  $\text{He}_{140}$ ). It also indicates that the reverse process of loop coalescence, i.e. loop dissociation, is almost impossible to be observed within the timescale accessible to atomistic simulations.

Thermal fluctuations determine that the critical events underlying He cluster growth exhibit a stochastic manner and possibly there is more than one low energy reaction pathway for these events. We should remark that obtaining the energy landscape of trap mutation and loop punching events is beyond the capability of present work due to that these reactions are triggered by the highly mobile He atoms and their complex rearrangements, which makes it difficult to obtain

reliable reaction pathways. Nevertheless, the kinetic barriers of this process are expected to be very low [36], especially when the He cluster gets larger ( $< 0.5$  eV for  $\text{He}_n$  ( $n > 8$ ) cluster)). Additionally, we should point out that factors such as temperature, cluster growth rate and interatomic potential are not taken into account here. For example, Sandoval *et al* [8] suggested that the spatial correlation of SIAs around the He cluster depends very much on its growth rates. Therefore, altering the growth rate by orders of magnitude might lead to different SIA distributions. Future works are in progress to further probe the synergistic effect of these factors on He cluster nucleation and growth in W.

In summary, we have revealed the energetics and kinetics on He cluster growth in bcc W using combined simulation techniques. The key mechanisms contributing to the decrease of system potential energy are trap mutation,  $\langle 100 \rangle \rightarrow 1/2\langle 111 \rangle$  cluster transformation, loop punching, loop coalescence and loop capturing. The formation of the metastable small  $\langle 100 \rangle$  cluster attached to the He cluster was initially observed in the trap mutation process. It subsequently transformed to the more energetically favorable  $1/2\langle 111 \rangle$  cluster. Two differently oriented  $1/2\langle 111 \rangle$  loops punched out by the over-pressurized

He cluster can readily react and coalesce (smaller loop rotated into the orientation of the larger loop) within the timescale of MD simulations. We also present the observation of an unusual loop capturing event possibly arising due to the strong loop attraction. This novel mechanism, yet to be validated by experimental and theoretical studies, is expected to be observed at a wide range of temperatures due to the high mobility of SIA loops. Furthermore, according to our estimation, the kinetic barriers associated with these key events are estimated to very low (no more than 0.5 eV). The present results indicate that the physical processes involved in the He cluster nucleation and growth in metals are far more complicated than traditionally assumed. The energetics and kinetics analysis method employed in this study can be transposed to investigating the critical events of He cluster evolution in systems containing extended defects such as dislocation, grain boundary and surface, in which case, a direct connection between atomistic simulations and experimental observations (e.g. surface fuzz growth) can be established.

## Acknowledgment

This work is supported by the National Magnetic Confinement Fusion Program with Grant No. 2013GB109002 and the National Natural Science Foundation of China with Grant No.51171008.

## References

- [1] Wilson W.D., Bisson C.L. and Baskes M.I. 1981 *Phys. Rev. B* **24** 5616
- [2] Seletskaya T., Osetsky Y., Stoller R.E. and Stocks G.M. 2008 *Phys. Rev. B* **78** 134103
- [3] Henriksson K.O.E., Nordlund K., Krasheninnikov A. and Keinonen J. 2005 *Appl. Phys. Lett.* **87** 163113
- [4] Becquart C.S. and Domain C. 2006 *Phys. Rev. Lett.* **97** 196402
- [5] Yang L., Zu X.T., Xiao H.Y., Gao F., Heinisch H.L., Kurtz R.J. and Liu K.Z. 2006 *Appl. Phys. Lett.* **88** 091915
- [6] Sefta F., Hammond K.D., Juslin N. and Wirth B.D. 2013 *Nucl. Fusion* **53** 073015
- [7] Lasa A., Tähtinen S.K. and Nordlund K. 2014 *Europhys. Lett.* **105** 25002
- [8] Sandoval L., Perez D., Uberuaga B.P. and Voter A.F. 2015 *Phys. Rev. Lett.* **114** 105502
- [9] Zhou H.-B., Liu Y.-L., Jin S., Zhang Y., Luo G.-N. and Lu G.-H. 2010 *Nucl. Fusion* **50** 115010
- [10] Becquart C.S. and Domain C. 2009 *J. Nucl. Mater.* **386–8** 109
- [11] Yang L., Gao F., Kurtz R.J. and Zu X.T. 2015 *Acta Mater.* **82** 275
- [12] Lucas G. and Schäublin R. 2008 *J. Phys.: Condens. Matter* **20** 415206
- [13] Zhang L., Fu C.-C. and Lu G.-H. 2013 *Phys. Rev. B* **87** 134107
- [14] Ullmaier H. 1984 *Nucl. Fusion* **24** 1039
- [15] Trinkaus H. and Singh B.N. 2003 *J. Nucl. Mater.* **323** 229
- [16] Kajita S., Takamura S., Ohno N., Nishijima D., Iwakiri H. and Yoshida N. 2007 *Nucl. Fusion* **47** 1358
- [17] Smirnov R.D. and Krasheninnikov S.I. 2013 *Nucl. Fusion* **53** 082002
- [18] Baldwin M.J. and Doerner R.P. 2008 *Nucl. Fusion* **48** 035001
- [19] Wright G.M., Brunner D., Baldwin M.J., Doerner R.P., Labombard B., Lipschultz B., Terry J.L. and Whyte D.G. 2012 *Nucl. Fusion* **52** 042003
- [20] Kajita S., Sakaguchi W., Ohno N., Yoshida N. and Saeki T. 2009 *Nucl. Fusion* **49** 095005
- [21] Miyamoto M., Watanabe T., Nagashima H., Nishijima D., Doerner R.P., Krasheninnikov S.I., Sagara A. and Yoshida N. 2014 *Phys. Scr.* **2014** 014028
- [22] Fiflis P., Curreli D. and Ruzic D.N. 2015 *Nucl. Fusion* **55** 033020
- [23] Lhuillier P.E., Belhabib T., Desgardin P., Courtois B., Sauvage T., Barthe M.F., Thomann A.L., Brault P. and Tessier Y. 2013 *J. Nucl. Mater.* **433** 305
- [24] Gao N., Victoria M., Chen J. and Swygenhoven H.V. 2011 *J. Phys.: Condens. Matter* **23** 245403
- [25] Thomas G.J. and Bastasz R. 1981 *J. Appl. Phys.* **52** 6426
- [26] Wang J., Hou Q., Sun T., Long X., Wu X. and Luo S. 2007 *J. Appl. Phys.* **102** 093510
- [27] Gao N., Swygenhoven H.V., Victoria M. and Chen J. 2011 *J. Phys.: Condens. Matter* **23** 442201
- [28] Sefta F., Juslin N. and Wirth B.D. 2013 *J. Appl. Phys.* **114** 243518
- [29] Plimpton S. 1995 *J. Comput. Phys.* **117** 1
- [30] Juslin N. and Wirth B.D. 2013 *J. Nucl. Mater.* **432** 61
- [31] Nosé S. 1984 *J. Chem. Phys.* **81** 511
- [32] Hoover W.G. 1985 *Phys. Rev. A* **31** 1695
- [33] Martyna G.J., Klein M.L. and Tuckerman M. 1992 *J. Chem. Phys.* **97** 2635
- [34] Stukowski A. 2010 *Modelling Simul. Mater. Sci. Eng.* **18** 015012
- [35] Evans J.H., van Veen A. and Caspers L.M. 1981 *Nature* **291** 310
- [36] Boisse J., Domain C. and Becquart C.S. 2014 *J. Nucl. Mater.* **455** 10
- [37] Henriksson K.O.E., Nordlund K. and Keinonen J. 2006 *Nucl. Instrum. Methods Phys. Res. B* **244** 377
- [38] Xu H., Stoller R.E., Osetsky Y.N. and Terentyev D. 2013 *Phys. Rev. Lett.* **110** 265503
- [39] Marian J., Wirth B.D. and Perlado J.M. 2002 *Phys. Rev. Lett.* **88** 255507
- [40] Henkelman G., Uberuaga B.P. and Jónsson H. 2000 *J. Chem. Phys.* **113** 9901